Features of near-inertial motions observed on the northern South China Sea shelf during the passage of two typhoons

CHEN Shengli[1], HU Jianyu[1*], POLTON Jeff A.[2]

[1]State Key Laboratory of Marine Environmental Science, College of Ocean & Earth Sciences, Xiamen University, Xiamen 361102, China

[2]National Oceanography Centre, 6 Brownlow Street, Liverpool L3 5DA, UK

* Corresponding author, Email: hujy@xmu.edu.cn

Abstract:

Features of near-inertial motions on the shelf (60 m deep) of northern South China Sea were observed under the passage of two typhoons during the summer of 2009. There are two peaks in spectra at both sub-inertial and super-inertial frequencies. The super-inertial energy maximizes near the surface, while the sub-inertial energy maximizes at a deeper layer of 15 m. The sub-inertial shift of frequency is induced by the negative background vorticity. The super-inertial shift is probably attributed to the near-inertial wave propagating from higher latitudes. The near-inertial currents exhibit a two-layer pattern being separated at mid-depth (25~30 m), with the phase in the upper layer being nearly opposite to that in the lower layer. The vertical propagation of phase implies the near-inertial energy is not dominantly downward. The upward flux of near-inertial energy is more evident at the surface layer (<17 m). There exist two boundaries at 17 m and 40 m, where the near-inertial energy is reflected upward and downward. The near-inertial motion is intermittent and can reach a peak of as much as 30 cm/s. The passage of Typhoon Nangka generates an intensive near-inertial event, but Typhoon Linfa does not. This difference is attributed to the relative mooring locations, which is on the right hand side of Nangka's path (leading to a wind pattern rotating clockwise with time) and is on the left hand side of Linfa's path (leading to a wind pattern rotating anti-clockwise with time).

Keywords: near-inertial motions, typhoon, South China Sea

1. Introduction

Near-inertial motion has been commonly observed over an extensive range of latitudes and depths in the ocean (Webster, 1965). It is mainly generated by wind (e.g. Pollard, 1970; Pollard and Millard, 1970). The passage of a front, a storm or a tropical cyclone can usually produce strong near-inertial motions in the ocean (e.g. D'Asaro, 1985), with a speed peak usually over 30 cm/s and with a decay time scale of more than 5 days (e.g. Brooks, 1983; Chen et al., 1996).

A one-year observation on the New England Shelf indicates that the current variance in near-inertial band comprises 10~20% of the total current variance (Shearman, 2005). In summer time, shelf sea near-inertial motion usually displays a two-layer structure, with the current in the upper layer opposite to that in the lower layer (e.g. MacKinnon and Gregg, 2005; Chen et al., 1996). This two-layer structure can form a strong current shear across thermocline, which is related to high dissipation (e.g. Burchard and Rippeth, 2009).

In shelf seas, several dynamic processes usually coexist and interact with near-inertial motions. The nonlinear interaction between inertial motions (frequency f) and internal tides (frequency ω) can produce energy at the superposition $f + \omega$ frequency (Xing and Davies, 2002). Similarly, the frequency of inertial motions can be shifted by the background vorticity to create an effective frequency, leading to the region of wave trapping or propagation (Kunze, 1985). Note in particular this vorticity effect is associated with the background dynamics (e.g. the presence of a front, a mesoscale eddy, or a shear of the background mean flow). Therefore, the near-inertial motion usually exhibits some local properties particular to the local dynamics of the background flow.

In the South China Sea, there have been a number of researches on near-inertial motions. The typhoon that frequently happens in summer can generate strong near-inertial motions, which can last for 1-2 weeks and have a current peak over 50 cm/s (e.g. Chen, 2006; Zhu and Li, 2007; Sun Z. et al., 2011). However, there is clear seasonal variability with the greatest near-inertial energy intensity in autumn (August, September and October, Chen et al., 2013). Near-inertial energy is mostly baroclinic (Liang et al, 2005), and could induce turbulent mixing and chlorophyll-*a* enhancement (Zhang et al., 2014). The blue-shift (Sun L. et al., 2011) or red-shift (Sun Z. et al., 2011) of the local inertial frequency are observed and attributed to the background vorticity. Since the South China Sea spans a range of latitudes and dynamical

regions, the character of near-inertial motions may vary throughout the South China Sea. Many region specific characteristics have yet to be described.

In this paper, by analysing a mooring data deployed on the shelf of the northern South China Sea during the passage of two typhoons, several new characteristics of near-inertial motions are revealed. The data are described in Section 2. Section 3 presents primary analyses firstly on the spectra and near-inertial currents, and then further studies the vertical energy flux. The mechanism for the slight shift of inertial frequency and the role of wind on generation are discussed in Section 4. Section 5 makes a summary.

2. Data

A bottom mounted Acoustic Doppler Current Profiler (ADCP) was deployed on the shelf of northern South China Sea (Fig. 1) at a depth of 60 m. The location is 116º39.56ʹE, 22 º11.85ʹN. It measured currents for 23 days from 14 June to 6 July in 2009 every 5 minutes. The vertical sampling interval is 2 m, ranging from a depth of 6 m to 48 m. During its working period, Typhoon Linfa and Typhoon Nangka passed through the region.
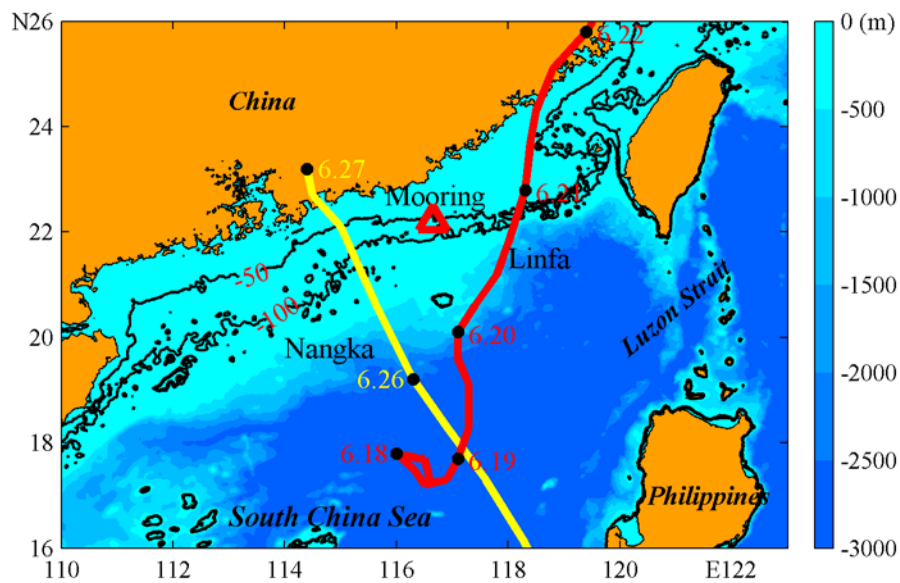

Fig. 1. Bathymetry map of the northern South China Sea. An ADCP mooring (triangle) is deployed in 60 m during the summer of 2009. The yellow and red lines represent the tracks of typhoons Nangka and Linfa, respectively. The black dots along the tracks denote 0:00 o'clock for the dates shown as 'month.day'. Black contours show 50 m and 100 m isobaths.

3. Results

3.1 Primary Analysis

A spectral analysis is first applied to the time series of each velocity component (eastward, u, and northward, v) separately, as shown in Fig. 2. The mooring is located at the latitude of 22 °11.85´N, corresponding to an inertial frequency of 0.76 cycles per day (i.e. 31.76 hours in period) which is denoted by a pink line in Fig. 2. A significant spectra peak occurs at a frequency slightly lower than the inertial frequency (denoted by 'sub-inertial' hereafter). It is interesting that another peak also occurs at the frequency higher than the inertial frequency (denoted by 'super-inertial' hereafter), although this peak is weaker than the sub-inertial peak. Both sub- and super-inertial peaks have a double-maximum in the vertical, with the high value in the upper layer being greater than that in the lower layer. However, the super-inertial energy is maximal near the surface, which is a commonly observed vertical structure for near-inertial motions (e.g. Shearman 2005; Zheng et al., 2006), whereas the sub-inertial energy is maximal at a deeper level of 15 m. Previous observations in this region only show a sub-inertial peak (Sun Z. et al., 2011). The mechanism for these two peaks will be discussed in Section 4.1.
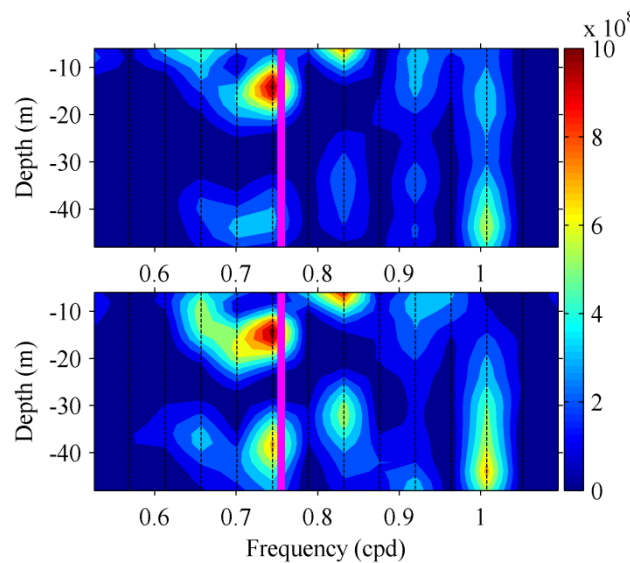

Fig. 2. Spectra (cm^2/s^2) of velocity components in near-inertial bands. The upper panel shows the eastward velocity component (u). The lower panel shows the northward velocity component (v). The pink line denotes the local inertial frequency. Dashed lines represent the maximum resolution of frequency in the spectral analysis.

A band pass filter is applied to obtain the near-inertial currents, preserving the currents at both the sub-inertial and the super-inertial frequencies (0.60~0.85 cpd). As seen from Fig. 3, near-inertial currents are most energetic between the 27th June and the 2nd July, reaching as much as 30 cm/s. During this period, the velocity in the upper layer (<25 m) is in the opposite direction to that in the lower layer (>30 m), for

both u and v components. An apparent boundary is present at around mid-depth. Such a two-layer structure has been frequently reported for near-inertial currents (e.g. Malone, 1968; Millot and Crepon, 1981; Mirko, 1987). It is commonly attributed to the no normal flow condition at a coastline (e.g. Millot and Crepon, 1981; Chen et al., 1996; Xing et al., 2004), which requires that the mass fluxes in the upper and lower layers are of the same magnitude, but in opposite direction. Between the 15th and 20th of June, the two-layer structure is also apparent, and the position of the mid-depth boundary shoals gradually with time. After the 2nd July, the water column behaves like a three-layer structure in u, and irregularly in v. The vertical structure of near-inertial motions evolves under influence of the stratification (e.g. Shearman, 2005) and the bottom stress (MacKinnon and Gregg, 2005). This evolution, though interesting, cannot be investigated further without density profile measurements.
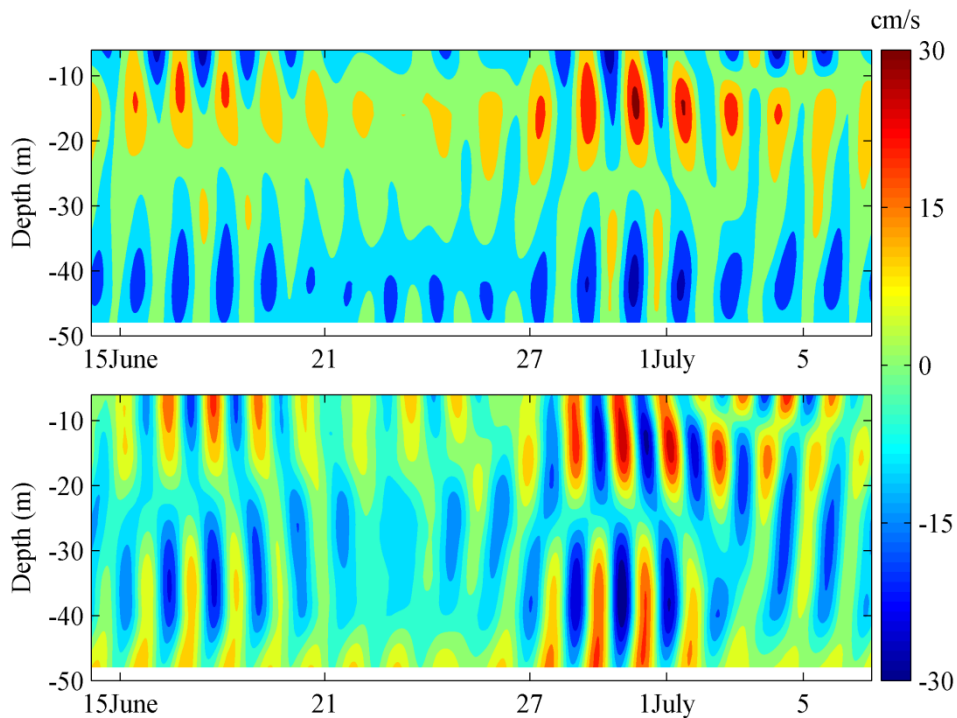

Fig. 3. Near-inertial currents obtained by band-pass filtering. Upper panel—eastward velocity (u); Lower panel—northward velocity (v). The date number on the x-axis denotes 0:00hr for the respective day.

3.2 Vertical Propagation of Phase and Energy

For the period of strong near-inertial motions between the 26th of June and the 2nd of July, the phase of near-inertial currents is contoured in Fig. 4, where the phase is defined to increase clockwise. Elsewhere the dominant energy flux of near-inertial motions is reported to be downward (e.g. Sanford, 1975; Leaman,

1975; Fu, 1981; van Haren, 2006), as observed in terms of an upward propagation of phase (e.g. Sun Z. et al., 2011). However, in this record the upward propagation of phase is not dominant. Indeed in the upper layer (<25 m), the downward propagation clearly dominates (upward propagation does briefly occur around the 27th of June). In the lower layer (>25 m), the upward propagation is intermittent with intervals of little vertical propagation.
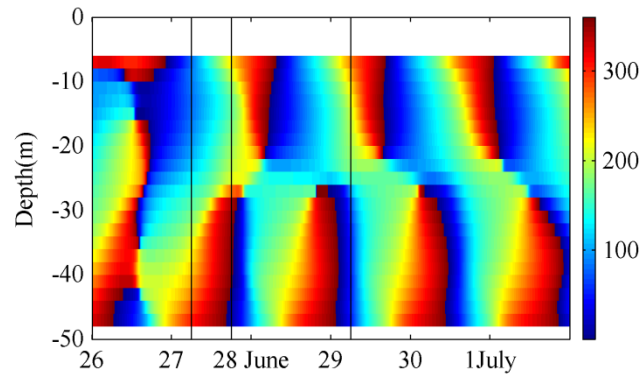

Fig. 4. The phase (degrees) of the near-inertial current. The phase of northward current is denoted by zero, increasing in the clockwise direction. Three vertical lines denote profiles that are further analysed.

To get more understanding, we investigate three typical profiles. At 06:00 on the 27th of June (Fig. 5a), the velocity vectors rotate clockwise with depth, indicating an upward propagation of phase, and thus a downward flux of near-inertial energy. At 18:00 on the 27th of June (Fig. 5b), the velocity vectors rotate counter-clockwise with depth near the surface, then exhibit a complicated clockwise and then counter-clockwise rotation towards the bed. At 06:00 29 June (Fig. 5c), the rotation is clearly counter-clockwise at the upper layer, and turns little in the lower layer.
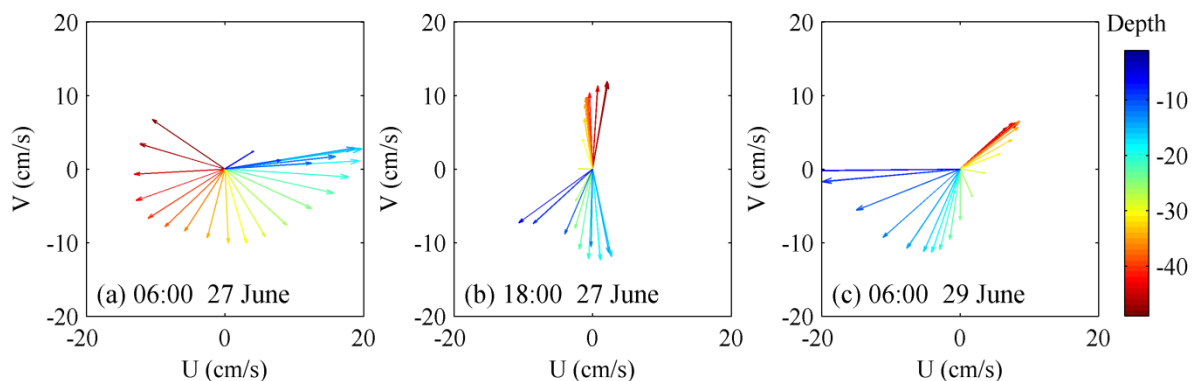

Fig. 5. Profiles of the near-inertial velocity vectors at a) 06:00 on 27 June; b) 18:00 on 27 June; c) 06:00 on 29 June, as depicted in Fig. 4.

The vertical propagation of near-inertial energy can be calculated at each depth using the vertical phase gradient (Fig. 6). On the 28th of June, the energy flux is downward at most depths. This is at the start of the near-inertial event, which as it evolves two boundary layers emerge (at 17m and 40m) that are associated with alternating upward and downward fluxes of near-inertial energy. The energy may penetrate through these boundaries. Such a vertical structure of near-inertial energy flux has not been reported previously.
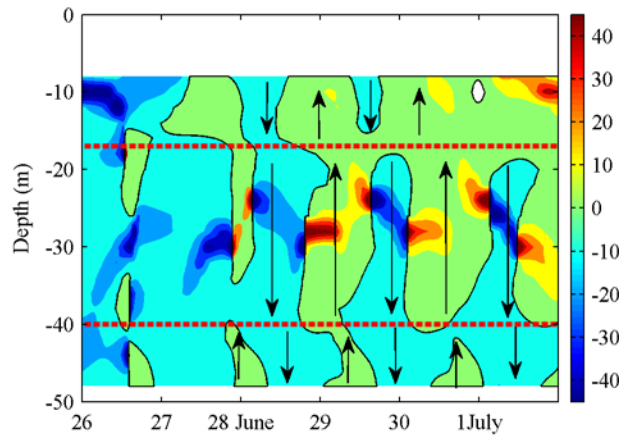

Fig. 6. The vertical phase gradient (degree/m) of near-inertial velocities. The positive value represents the greater phase at deeper position, indicating upward propagation of phase, thus downward flux of energy. The negative value represents upward flux of energy. The black line denotes zero value, the red dash lines are the probable reflection boundaries, the black arrows indicate the direction of energy flux.

4. Discussion

4.1 Frequency Shift

As seen in Fig. 2, the energy peaks appear at both sub-inertial and super-inertial frequencies. This phenomenon has been rarely reported. Given their different vertical structures as described in Section 3.1, it is possible that they are of different near-inertial events.   Figure 7 shows the variability of the kinetic energy at these two frequencies. Before the 25th of June, they are of similar value and both decline gradually with time. After this date, the sub-inertial energy rises sharply and then rapidly diminishes, while the super-inertial energy only experiences a slight increase. This suggests the sub-inertial and super-inertial energy are not completely uncorrelated and independent with each other, since they share some similarity in tendency.
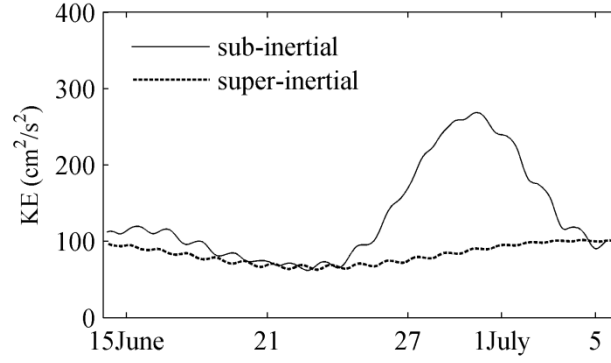
Fig. 7. The kinetic energy (cm^2/s^2) at the sub-inertial and super-inertial frequencies. The currents at sub-inertial and super-inertial frequencies obtained by band-pass filter are applied to compute the kinetic energy at each depth, and then averaged vertically and over the inertial period.

When there is a horizontal shear in the background flow, the resultant vorticity can alter the frequency of inertial motions to induce a slight departure from the inertial frequency. In such instances, the near-inertial motion acquires an effective frequency (Kunze, 1985), given by Eq. (1), where f_{eff} is the effective frequency, f is the local inertial frequency, and ζ is the background vorticity. Indeed the sub-inertial energy reported by Sun Z. et al. (2011) in the same region is attributed to this frequency shift mechanism.

$$f_{eff} \approx \sqrt{f(f+\zeta)} \approx f + \frac{\zeta}{2} = f + \frac{1}{2}\left(\frac{\partial v}{\partial x} - \frac{\partial u}{\partial y}\right) \qquad (1)$$

Using the surface current data (u and v in Eq. 1) obtained from NOAA satellite data set OSCAR with a resolution of 1/3 degree (http://www.oscar.noaa.gov/), the background vorticity is computed. As seen from Fig. 8, the negative background vorticity always shifts the frequency to be smaller than the inertial frequency (referred as sub-inertial shift hereafter). The sub-inertial shift is enhanced with time. Between 27 June and 2 July when the near-inertial motion is most energetic, the effective frequency is around 90% of local inertial frequency, generally consistent with the situation in the spectrum of velocities (Fig. 2). This is highly suggestive that the sub-inertial shift is induced by the negative background vorticity. The sub-inertial wave is trapped by the negative vorticity and cannot propagate laterally (Kunze, 1985), thus only propagate downward. This explains the unusual sub-surface intensified structure of the sub-inertial spectra.
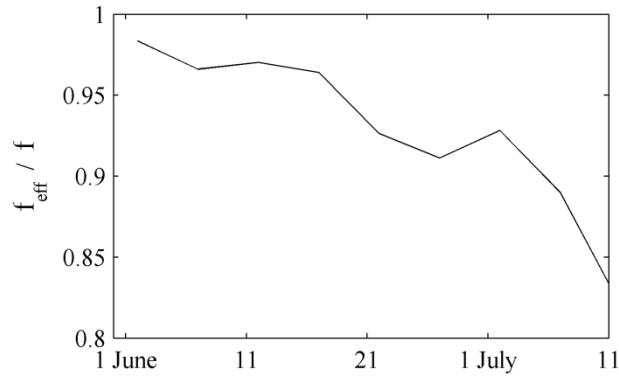
Fig. 8. The effective frequency induced by background vorticity of the flow.

Indeed the super-inertial motion would be expected to have been subject to the same frequency shift. The super-inertial motion is likely to have been generated as a near-inertial wave at a more poleward latitude which has propagated into this region (Fu, 1981), whereas the sub-inertial motion is likely to have been generated locally. If it is generated at a latitude higher enough, the negative vorticity is insufficient to shift its frequency toward being sub-inertial. It is hard to assess what its original frequency might have been before the shifting occurred. Nevertheless it is clear that this slight frequency shift by the background vorticity field would be insufficient to trap the super-inertial wave.

4.2 Generation by Wind

Near-inertial motions are mainly wind-driven (e.g. Pollard, 1970; Pollard and Millard, 1970). In particular, strong near-inertial currents can be generated by a typhoon's passage (e.g. Zhu and Li, 2007; Sun Z. et al., 2011). Figure 9a shows the temporal variation of depth-averaged near-inertial kinetic energy. It is greatest between the 27th of June and the 2nd of July, and weakest between the 21st-25th of June.

Figures 9b and c display a wind time series at a location near the mooring site, obtained from the satellite data Cross-Calibrated Multi-Platform (CCMP, podaac.jpl.nasa.gov/DATA_CATALOG/ccmpinfo.html) (Atlas et al., 2011). Two peaks in wind speed, of almost 15 m/s, occur on the 21st and 27th of June, which are induced by typhoons Linfa and Nangka respectively. Following the passage of Nangka, the near-inertial energy increases gradually and reaches a significant peak. However, after the passage of Linfa (after 22 June) the near-inertial energy shows no significant increase, but instead diminishes to its smallest value during this record.
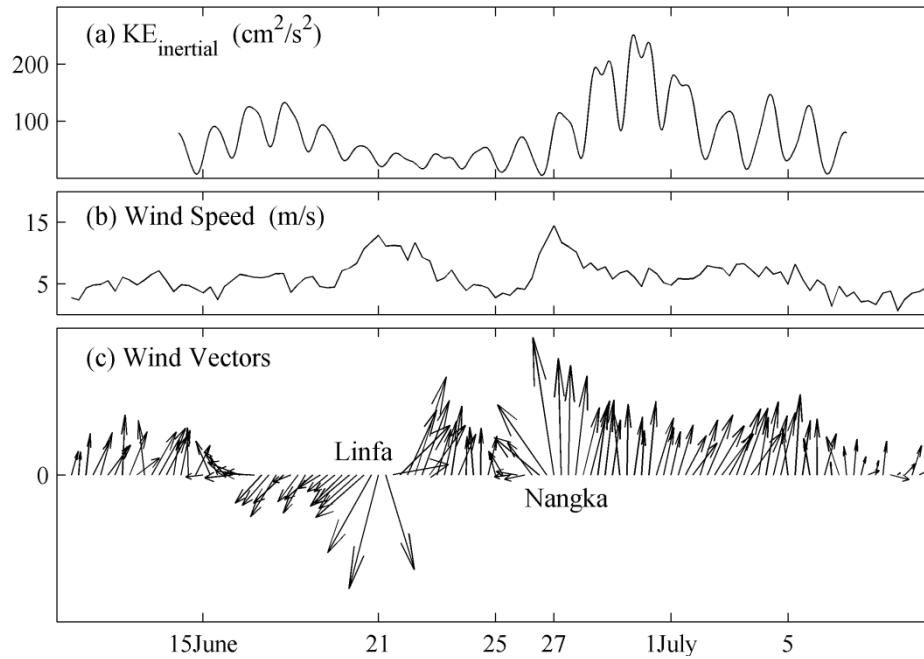
Fig. 9. (a) The kinetic energy of near-inertial current, and the wind speed (b) and wind vectors (c) near the mooring. The kinetic energy is computed firstly from near-inertial currents, and then averaged over the depth. The wind data comes from the satellite data set Cross-Calibrated Multi-Platform (CCMP), with a spatial resolution of 0.25 degree and a time interval of 6 hours.

Price (1981) pointed out that, for a fixed location on the right hand side of cyclone's heading direction, the wind rotates clockwise with time, while for a fixed location on the left hand side the wind rotates anti-clockwise (see detailed interpretation in Fig. 10). In northern hemisphere, the near-inertial motion is clockwise and thus clockwise wind can resonantly force near-inertial motions, in contrast to anti-clockwise winds. It is for this reason that the near-inertial motion generated at a fixed location on the right hand side along the typhoon path is more intensive (Price, 1981). This effect is clearly apparent in these data. The mooring site is on the right hand side of the Nangka's path, while it is on the left hand side of the Linfa's path. Therefore, Nangka's passage drives a wind pattern rotating clockwise with time (Fig. 9c) and generates an intense near-inertial event. On the other hand, Linfa's passage generates an anti-clockwise wind pattern (Fig. 9c), and does not promote the near-inertial motion.
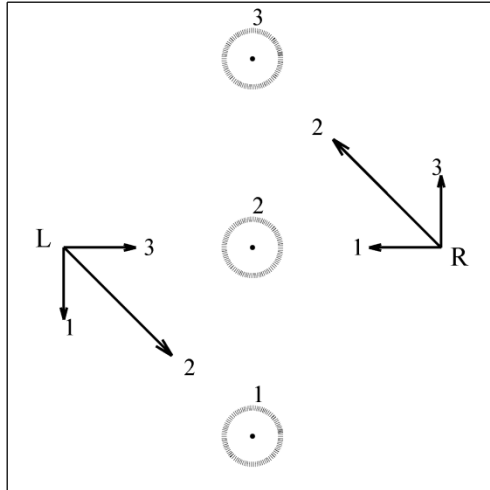
Fig. 10. Diagram of different wind patterns along a cyclone's path. The circles with points at the centre represent the cyclone as it moves northward from position 1 to 3. The corresponding wind at the position R, i.e. on the right hand side, rotates clockwise with time from 1 to 3. The wind at the position L, i.e. n the left hand side, roatates anti-clockwise with time. The radial and tangential wind stress is assumed to be equal.

5. Summary

An ADCP mooring was deployed on the shelf of northern South China Sea at a depth of 60 m. It operated for 23 days during the summer of 2009, during which Typhoon Linfa and Typhoon Nangka passed through.

The spectrum of measured currents shows two significant peaks near the local inertial frequency. One is slightly lower (sub-inertial) and the other is higher (super-inertial) than the local inertial frequency. The sub-inertial peak is more energetic than the super-inertial one, and has a broader frequency band. They both display a two-layer structure, with two maxima in vertical. However, the super-inertial energy maximizes near the surface (as is a normally observed structure), while the maximum of the sub-inertial energy is found deeper at around 15 m depth. Previous research in this region only reports sub-inertial energy. The surface current obtained from satellite data indicates a patch of negative vorticity that shifts the inertial motion to become sub-inertial and traps the near-inertial motion, thus resulting the sub-surface intensification. The super-inertial energy probably originates as a near-inertial wave generated at a more poleward latitude.

A band pass filtering is applied to extract the near-inertial currents. They behave as a two-layer structure in the vertical, with a layer of minimum value at mid-depth. The velocity phase in the upper layer is nearly

opposite to that in the lower layer. This vertical structure, probably correlated with the stratification structure, evolves with time. The vertical distribution of phase shows that an upward propagation of phase, i.e. indicating a downward flux of near-inertial energy, is not as dominant as has been previously reported. The vertical gradient of phase is used to denote the direction of vertical near-inertial energy flux. There seems to be two boundaries at 17 m and 40 m, where the energy is reflected upward and downward. This is a new phenomenon that deserves further investigation.

The intensity of the near-inertial currents is time dependent and greatest during the influence of Typhoon Nangka, when it reaches high as 30 cm/s. This is because the wind forcing is resonant as the mooring is on the right hand side along Nangka's path. This effect is highlighted in stark contrast to the passage of Typhoon Linfa, along whose path the mooring is on the left hand side and has no discernable elevation in near-inertial energy.

References

Atlas R, Hoffman R N, Ardizzone J, et al. 2011. A cross-calibrated, multiplatform ocean surface wind velocity product for meteorological and oceanographic applications. Bull Amer Meteor Soc, 92: 157-174

Burchard H, Rippeth T P. 2009. Generation of bulk shear spikes in shallow stratified tidal seas. J Phys Oceanogr, 39: 969-985

Brooks D A. 1983. The wake of Hurricane Allen in the western Gulf of Mexico. J Phys Oceanogr, 13: 117-129

Chen C, Reid R O and Nowlin Jr W D. 1996. Near-inertial oscillations over the Texas-Louisiana shelf. J Geophys Res, 101: 3509 -3524

Chen K. 2006. Typhoon induced inertial motion in the South China Sea [dissertation]. Taiwan: National Taiwan University, 98

Chen G, Xue H, Wang D, et al. 2013. Observed near-inertial kinetic energy in the northwestern South China Sea. J Geophys Res, 118: 4965-4977

D'Asaro E A. 1985. The energy flux from the wind to near-inertial motions in the surface layer. J Phys Oceanogr, 15: 1043-1059

Fu L L. 1981. Observations and models of inertial waves in the deep ocean. Rev Geophys, 19: 141-170

Kundu P K. 1976. An analysis of inertial oscillations observed near Oregon coast. J Phys Oceanogr, 6: 879-893

Kunze E. 1985. Near-inertial wave propagation in geostrophic shear. J Phys Oceanogr, 15: 544-565

Leaman K D and Sanford T B. 1975. Vertical energy propagation of inertial waves: a vector spectral analysis of velocity profiles. J Geophys Res, 80: 1975-1978

Liang X, Zhang X and Tian J. 2005. Study on internal tides and near-inertial motions in the upper 450 m ocean in the northern South China Sea. Chin Sci Bull, 50: 2027-2031

MacKinnon J A and Gregg M C. 2005. Near-inertial waves on the New England shelf: the role of evolving stratification, turbulent dissipation, and bottom drag. J Phys Oceanogr, 35: 2408-2424

Malone F D. 1968. An analysis of current measurements in Lake Michigan. J Geophys Res, 73: 7065-7081

Millot C and Crepon M. 1981. Inertial oscillations on the continental shelf of the Gulf of Lions-observations and theory. J Phys Oceanogr, 11: 639-657

Mirko O. 1987. Oscillations of the inertia period on the Adriatic Sea shelf. Cont Shelf Re, 7: 577-598.

Pollard R T. 1970. On the generation by winds of inertial waves in the ocean. Deep Sea Res, 17: 795-812

Pollard R T and Millard R C. 1970. Comparison between observed and simulated wind-generated inertial oscillation, Deep Sea Res, 17: 813-821

Pollard R T. 1980. Properties of near-surface inertial oscillations. J Phys Oceanogr, 10: 385-398

Price J F. 1981. Upper ocean response to a hurricane. J Phys Oceanogr, 11: 153-175

Sanford T B. 1975. Observations of the vertical structure of internal waves. J Phys Oceanogr, 80: 3861-3871

Shearman R K. 2005. Observations of near-inertial current variability on the New England shelf. J Geophys Res, 110, C02012, doi: 10.1029/2004JC002341

Sun Z, Hu J, Zheng Q, et al. 2011. Strong near-inertial oscillations in geostrophic shear in the northern South China Sea. J Oceanogr, 67:377-384

Sun L, Zheng Q, Wang D, et al. 2011. A case study of near-inertial oscillation in the South China Sea using mooring observations and satellite altimeter data. J Oceanogr, 67: 677-687

van Haren H. 2006. Asymmetric vertical internal wave propagation. Geophys Res Lett, 33, L06618, doi:10.1029/2005GL025499

Webster F. 1968. Observations of inertial-period motions in the deep sea. Rev Geophys Space Phys, 6: 473-490

Xing J and Davies A M. 2002. Processes influencing the non-linear interaction between inertial oscillations, near inertial internal waves and internal tides. Geophys Res Lett, 29(5), 1067, doi: 10.1029/2001GL014199

Xing J, Davies A M and Fraunie P. 2004. Model studies of near-inertial motion on the continental shelf off northeast Spain: A three-dimensional/two-dimensional/one-dimensional model comparison study. J Geophys Res, 109, C01017, doi:10.1029/2003JC001822

Zhang S, Xie L, Hou Y, et al. 2014. Tropical storm-induced turbulent mixing and chlorophyll-a enhancement in the continental shelf southeast of Hainan Island. J Marine Syst, 129: 405-414

Zheng Q, Lai R J, Huang N E, et al. 2006. Observation of ocean current response to 1998 Hurricane Georges at Gulf of Mexico. Acta Oceanol Sin, 25:1-14

Zhu D and Li L. 2007. Near inertial oscillations in shelf break of northern South China Sea after passage of typhoon Wayne. J Trop Oceanogr, 26:1-7 (in Chinese with an English abstract)